

Data-Driven Robust Optimization using Unsupervised Deep Learning

Marc Goerigk^{*1} and Jannis Kurtz^{†2}

¹Network and Data Science Management, University of Siegen, Germany

²Management Science, University of Siegen, Germany

Abstract

Robust optimization has been established as a leading methodology to approach decision problems under uncertainty. To derive a robust optimization model, a central ingredient is to identify a suitable model for uncertainty, which is called the uncertainty set, containing all scenarios against which we wish to protect. An ongoing challenge in the recent literature is to derive uncertainty sets from given historical data.

In this paper we use an unsupervised deep learning method to construct non-convex uncertainty sets from data, which have a more complex structure than the typically considered sets. We show that the trained neural networks can be integrated into a robust optimization model by formulating the adversarial problem as a convex quadratic mixed-integer program. This allows us to derive robust solutions through an iterative scenario generation process. In extensive computational experiments, we compare this approach to a current state-of-the-art approach, which derives uncertainty sets by kernel-based support vector clustering. We find that uncertainty sets derived by the unsupervised deep learning method can give a better description of data, leading to robust solutions that considerably outperform the comparison method both with respect to objective value and feasibility.

1 Introduction

In many real-world optimization problems most of the observed parameters are uncertain which can be due to measurement or rounding errors, or since the true value is first revealed in the future. Examples of uncertain parameters can be future demands, unknown traffic situations, noisy data and many more. Therefore, there is a high demand for optimization models which can handle the occurring uncertainties. In contrast to stochastic approaches, the robust optimization approach is used to tackle optimization problems with uncertain parameters by a worst-case approach and needs no information about the underlying probability distribution of the uncertain parameters. More precisely, in robust optimization problems we typically want to find a solution which is feasible under all possible outcomes of the uncertain parameters and which is optimal in the worst-case. To this end the input of nearly all robust optimization models is an uncertainty set, which contains all possible outcomes of the uncertain parameters, called scenarios. One of the main questions arising in practical applications is which structure and size the uncertainty set should have.

^{*}marc.goerigk@uni-siegen.de, corresponding author

[†]jannis.kurtz@uni-siegen.de

Initialized by the seminal work of Soyster in 1973 [Soy73], the field of robust optimization fully emerged in the 1990s and was studied for several classes of uncertainty sets; including finite and convex uncertainty sets [KY96, BTEGN09, ABV09]. For convex uncertainty sets the most frequently used sub-classes are polyhedral, conic and ellipsoidal uncertainty sets [BTN98, BTN99, EGOL98, EGL97]. As a special case of polyhedral uncertainty the so-called budgeted uncertainty is a popular uncertainty class due to its simplicity and tractability [BS04, BS03]. Different uncertainty sets and their geometric relationship are studied in [LDF11]. Recently mixed uncertainty sets, combining most of the popular uncertainty classes into one set, were studied in [DGR20]. Next to the classical robust optimization approach, several less conservative approaches have been introduced. A survey about the classical and more recent robust optimization approaches for discrete and convex uncertainty can be found in [BK18].

The main question for a user, applying a robust optimization model, is how to choose the structure and the size of the uncertainty set. In most real-world situations the user only has a finite set of observations of the uncertain parameters from the past. Nevertheless, constructing a finite uncertainty set by these observations can lead to overly pessimistic robust solutions due to outliers in the data and since no structural properties of the data are exploited. Furthermore, the robust optimization approach with finite uncertainty sets is known to be hard to solve, even for easy classical combinatorial optimization problems with only two scenarios [KY96]. To tackle this problem, several data-driven robust optimization approaches have been studied. On the one hand uncertainty sets can be constructed by statistical methods using nonparametric estimators to model confidence regions [AB20], hypothesis tests [BGK18] or statistical learning theory [TR14]. In [HHL17] the authors approximate a high probability region by combinations of classical uncertainty sets and then use a simple data-splitting scheme to determine the size of the region. In [CH15, NY17] Dirichlet process mixture models are used to construct uncertainty sets which are given by a union of ellipsoids. Furthermore, in [NY17] computationally tractable uncertainty sets with a polyhedral structure are constructed and applied to adaptive robust optimization problems. Polyhedral uncertainty sets incorporating correlations between uncertain parameters are derived in [NY18] using principal component analysis and kernel smoothing. On the other hand, deterministic approaches were developed to construct a range of uncertainty sets which were applied to the shortest path problem under real-world traffic scenarios of the City of Chicago [CDG19]. Finally several approaches deploying machine learning models were presented. Clustering and supervised machine-learning approaches were used in [GGJ20]. In [SHY17, SY19] the authors derive a kernel-based support vector clustering model to construct polyhedral uncertainty sets.

In this work we apply and adapt the unsupervised deep classification model developed in [RVG⁺18] to construct uncertainty sets which are given by level sets of a norm-function applied to the output of deep neural networks and therefore have a complex structure which can be adjusted by the parameters of the underlying neural network. In Section 3 we show that the constructed sets are given by a finite union of convex subsets, each of them having a polyhedral structure intersected with a transformed norm inequality. In particular our uncertainty sets are not convex in general and do not fit into any of the well known uncertainty classes. Nevertheless, we prove that it is possible to optimize over these sets using a mixed-integer programming formulation, which means that the robust optimization problem can be solved by an iterative scenario generation procedure. In Section 4 we show that robust solutions based on sets constructed this way outperform the solutions based on polyhedral uncertainty sets constructed via the kernel-based support vector clustering approach from [SHY17].

2 Preliminaries

2.1 Notation

We define $[k] := \{1, \dots, k\}$ for each $k \in \mathbb{N}$ and $\mathbb{R}_+^n := \{x \in \mathbb{R}^n : x \geq 0\}$. The ℓ_p -norm of a vector $x \in \mathbb{R}^N$ is defined by $\|x\|_p := \left(\sum_{i \in [N]} x_i^p\right)^{\frac{1}{p}}$. For a matrix $A \in \mathbb{R}^{m \times n}$ we denote by a_i the i -th row and by A_j the j -th column of A . For a vector $v \in \mathbb{R}^N$ we denote by $\text{diag}(v)$ the $N \times N$ matrix which has diagonal entries v and zero-entries otherwise. For given matrices W^1, \dots, W^L of appropriate dimensions we define the product

$$\prod_{i=1}^L W^i := W^L W^{L-1} \dots W^1.$$

2.2 Robust Optimization

Consider the deterministic linear optimization problem

$$\begin{aligned} \min \quad & d^\top x \\ \text{s.t.} \quad & c^\top x \leq b \\ & x \in X \end{aligned} \tag{1}$$

where $d \in \mathbb{R}^N$ is a given cost vector, $X = \{x \in \mathbb{R}^N : Tx \leq e\}$ a polyhedron and $c \in \mathbb{R}^N$, $b \in \mathbb{R}$. Assume that the coefficient parameters of the constraint $c^\top x \leq b$ are uncertain, i.e. the vector c is not known precisely. In robust optimization we assume that an uncertainty set $U \subset \mathbb{R}^N$ is given, which contains all possible realizations of the vector c . The aim is then to calculate an optimal solution which is feasible for each realization in U , i.e. we want to solve the problem

$$\begin{aligned} \min \quad & d^\top x \\ \text{s.t.} \quad & c^\top x \leq b \quad \forall c \in U \\ & x \in X \end{aligned} \tag{2}$$

which is equivalent to the problem

$$\begin{aligned} \min \quad & d^\top x \\ \text{s.t.} \quad & \max_{c \in U} c^\top x \leq b \\ & x \in X. \end{aligned} \tag{3}$$

If more than one constraint is uncertain, a similar reformulation can be applied for each such constraint. For certain classes of convex uncertainty sets U , replacing $\max_{c \in U} c^\top x$ by its dual formulation, Problem (3) can be transformed to a deterministic problem of a certain class [BTEGN09]. If U is a polyhedral uncertainty set, (3) is equivalent to a linear program, while for ellipsoidal uncertainty sets it becomes a quadratically constrained problem.

Nevertheless, if U is non-convex, e.g. finite, then the dualization step is not possible in general. In this case Problem (2) can be solved by iteratively generating new worst-case scenarios in U and adding them to the problem. More precisely, we alternately calculate an optimal solution $x^* \in \{x \in X : \max_{c \in U'} c^\top x \leq b\}$ of Problem (2) for a finite subset $U' \subset U$ and afterwards a worst-case scenario

$$c^* \in \arg \max_{c \in U} c^\top x^* \tag{4}$$

which is then added to U' if $(c^*)^\top x^* > b$ holds. Otherwise, we stop with an optimal solution x^* .

Sometimes the special case of the robust optimization problem is studied where the uncertain parameters only appear in the objective function, which can be modeled by

$$\min_{x \in X} \max_{c \in U} c^\top x. \quad (5)$$

Nevertheless, all results from above also hold for Problem (5). Finally, note that we can equivalently replace U by its convex hull $\text{conv}(U)$ in Problems (2) and (5), since we are optimizing a linear function over U .

2.3 Unsupervised Learning

In unsupervised learning (also called anomaly detection or one-class classification), the task is to decide whether a given data point is a normal data point or if it is anomalous. To this end the aim is to train an appropriate model on a set of unlabeled training data, which is assumed to contain the normal data points, and extract structural information from this training set to distinguish normal data from anomalous data in the future. Often the idea behind one-class classification models is to find a minimal norm-ball in a certain feature space, such that all anomalous data points are lying outside of the ball. In the following we summarize two approaches, the first based on support vector clustering and the second using deep neural networks.

Given a set of data points $c^1, \dots, c^m \in \mathbb{R}^N$ and a mapping $\phi : \mathbb{R}^N \rightarrow \mathbb{R}^K$ to a possibly high-dimensional feature space, the idea of soft margin support vector clustering (SVC) is to find the smallest sphere that encloses most of the training data, which can be done by solving the problem

$$\begin{aligned} \min \quad & R^2 + \frac{1}{N\nu} \sum_{i=1}^m \xi_i \\ \text{s.t.} \quad & \|\phi(c^i) - \bar{c}\|_2^2 \leq R^2 + \xi_i \quad i = 1, \dots, m \\ & \bar{c} \in \mathbb{R}^K, \quad R \geq 0, \quad \xi \in \mathbb{R}_+^m. \end{aligned} \quad (6)$$

Note that the mapping $\phi(c^i)$ of a data point can lie outside of the sphere around \bar{c} with radius R in which case $\xi_i > 0$ in an optimal solution. The distance ξ_i of each point outside of the sphere is penalized in the objective function and the parameter $\nu \in [0, 1]$ can be used to adjust the fraction of data points which will lie outside of the optimal sphere. Problem (6) is a convex problem and by applying the KKT conditions we obtain its dual problem

$$\begin{aligned} \min \quad & \sum_{i,j=1}^m \alpha_i \alpha_j K(c^i, c^j) - \sum_{i=1}^m \alpha_i K(c^i, c^i) \\ \text{s.t.} \quad & 0 \leq \alpha_i \leq \frac{1}{N\nu} \quad i \in [m] \\ & \sum_{i \in [m]} \alpha_i = 1, \end{aligned} \quad (7)$$

where $K(\cdot, \cdot)$ is a kernel function and $K(c^i, c^j) = \phi(c^i)^\top \phi(c^j)$. If K is a positive definite kernel, Problem (7) is a convex quadratic problem and can be solved by classical QP methods [BBV04] or due to its specific structure by the sequential minimal optimization procedure [ZYG⁺08].

The main idea in [SHY17] is to construct uncertainty sets

$$\mathcal{U} = \{c \in \mathbb{R}^N : \|\phi(c) - \bar{c}\|_2^2 \leq R^2\},$$

where \bar{c} and R are given by an optimal solution of (6). The authors apply the kernel

$$K(u, v) := \sum_{i \in [m]} l_i - \|Q(u - v)\|_1$$

where Q is a weighting matrix containing covariance information from data and the l_i are specified values. They derive the uncertainty set

$$\begin{aligned} \mathcal{U}_\nu = \{c \in \mathbb{R}^N : \exists v_i \in \mathbb{R}^N \quad \forall i \in \text{SV} \\ \sum_{i \in \text{SV}} \alpha_i v_i^\top \mathbf{1} \leq \min_{i' \in \text{BSV}} \sum_{i \in \text{SV}} \alpha_i \|Q(c^{i'} - c^i)\|_1 \\ - v_i \leq Q(c - c^i) \leq v_i \quad \forall i \in \text{SV}\} \end{aligned} \quad (8)$$

where α is the optimal solution of Problem (7), $\text{SV} := \{i : \alpha_i > 0\}$ is the set of support vectors and $\text{BSV} := \{i : \frac{1}{N_\nu} > \alpha_i > 0\}$ is the set of boundary support vectors. Geometrically, SV contains all indices of the data points which lie outside or on the boundary of the sphere, while BSV contains only the data points on the boundary. Note that the number of variables in the description of \mathcal{U}_ν depends on the number of support vectors and therefore grows with increasing sample size m and decreasing ν .

In [RVG⁺18] the authors study Problem (6) where $\phi(c)$ is replaced by the output of a neural network for data point c . A neural network is a function $f_{W^1, \dots, W^L} : \mathbb{R}^N \rightarrow \mathbb{R}^{d_L}$ which maps a data point $c \in \mathbb{R}^N$ to an output vector

$$f_{W^1, \dots, W^L}(c) = \sigma^L (W^L \sigma^{L-1} (W^{L-1} \dots \sigma^1 (W^1 c) \dots))$$

where $W^l \in \mathbb{R}^{d_l \times d_{l-1}}$ are the weight matrices, and $\sigma^l : \mathbb{R} \rightarrow \mathbb{R}$ for each $l \in [L]$ are activation functions which are applied component-wise. The dimension d_l is called the *width* of the l -th layer with $d_0 := N$. We define $W := (W^1, \dots, W^L)$. The authors represent a solution to the *One-Class Deep Support Vector Data Description* (Deep SVDD), which is given by the problem

$$\min_{W^1, \dots, W^L} \frac{1}{m} \sum_{i \in [m]} \|f_{W^1, \dots, W^L}(c^i) - \bar{c}\|_2^2 + \frac{\lambda}{2} \sum_{l \in [L]} \|W^l\|_F^2 \quad (9)$$

where \bar{c} is a given center point, $\lambda \geq 0$ a given control parameter and $\|\cdot\|_F$ denotes the Frobenius norm. After optimizing Problem (9) the radius $R^2 > 0$ can be chosen e.g. as the $(1 - \varepsilon)$ -quantile of the radii $r_i^2 := \|f_{W^1, \dots, W^L}(c^i) - \bar{c}\|_2^2$ of the training data, i.e. the calculated sphere contains $(1 - \varepsilon) \cdot 100\%$ of the training data. The center point \bar{c} is set to the average over all outputs of the training data by a neural network where the weights have the values of the first initialization of the stochastic gradient descent. The term $\frac{\lambda}{2} \sum_{l \in [L]} \|W^l\|_F^2$ is a regularizer which leads to smaller weights after training and which can be controlled by the parameter λ . A new data point $c \in \mathbb{R}^N$ is then classified as a normal scenario if $\|f_{W^1, \dots, W^L}(c) - \bar{c}\|_2 \leq R$. We will use this model in the next section to create uncertainty sets which can be used for robust optimization problems.

3 Creating Uncertainty Sets via Unsupervised Deep Learning

In this section we derive non-convex uncertainty sets using level sets of trained neural networks, which are given as described in Section 2.3. We assume that all activation functions are piecewise affine functions, i.e. they are of the form

$$\sigma^l(w) := \alpha_i^l w + \gamma_i^l \quad \text{if } \underline{\beta}^{i,l} \leq w < \bar{\beta}^{i,l} \quad \forall i \in [k_l] \quad (10)$$

for all $l \in [L]$, where $\alpha_i^l \in \mathbb{R}$ are the given slopes, γ_i^l are the given y -intercepts, $k_l \in \mathbb{N}$ is the number of intervals and $\underline{\beta}^{i,l} < \bar{\beta}^{i,l}$ are the bounds of the intervals where $\bar{\beta}^{i,l} = \underline{\beta}^{i+1,l}$, $\underline{\beta}^{1,l} = -\infty$ and $\bar{\beta}^{k_l,l} = \infty$ for all $l \in [L]$. Note that if σ^l is a continuous function, then we may also write $w \leq \bar{\beta}^{i,l}$ instead of $w < \bar{\beta}^{i,l}$. If all possible data points are contained in a bounded set and if the neural network is already trained, then we can replace ∞ by a large enough value $M > 0$. Note that the ReLU activation function $\sigma(w) = \max\{w, 0\}$ can be modeled by (10) setting $k_l = 2$, $\alpha_1^l = 0$, $\alpha_2^l = 1$, $\gamma_1^l = \gamma_2^l = 0$, $\underline{\beta}^{1,l} = -\infty$, $\bar{\beta}^{1,l} = 0$, $\underline{\beta}^{2,l} = 0$ and $\bar{\beta}^{2,l} = \infty$. Other piecewise affine activation functions as the Hardtanh or the hard sigmoid function can be modeled by (10) as well. In general, any continuous function could be approximated by these piecewise affine functions.

For a neural network, trained on the training sample $c^1, \dots, c^m \in \mathbb{R}^N$, and given by its weight matrices $W = (W^1, \dots, W^L)$, a center point $\bar{c} \in \mathbb{R}^{d_L}$ and a radius $R > 0$, we define the uncertainty set

$$U_f(W, \bar{c}, R) := \{c \in \mathbb{R}^N : \|f_{W^1, \dots, W^L}(c) - \bar{c}\| \leq R\} \quad (11)$$

for an arbitrary norm $\|\cdot\|$. Using the Deep SVDD method defined in (9) to train the neural network, the natural choice of $U_f(W, \bar{c}, R)$ would be given by using the Euclidean norm and the center point \bar{c} returned by the model. As noted in Section 2.3, the radius R can be chosen as the $(1 - \varepsilon)$ -quantile of the radii $r_i = \|f_{W^1, \dots, W^L}(c^i) - \bar{c}\|_2$ of the training data. Note that in this case if we calculate a solution of the robust constraint

$$c^\top x \leq b \quad \forall c \in U_f(W, \bar{c}, R)$$

this solution is also feasible for the *sample average approximation (SAA) chance constraint*

$$\mathbb{P}(\tilde{c}^\top x \leq b) \geq 1 - \varepsilon$$

where \tilde{c} has discrete and finite support and $\mathbb{P}(\tilde{c} = c^i) = \frac{1}{m}$ for each $i \in [m]$; see [PAS09] for more details on SAA.

In the following we define

$$\mathcal{A} := \left\{ u := (u^{i,l})_{l \in [L], i \in [k_l]} : u^{i,l} \in \{0, 1\}^{d_l}, \sum_{i \in [k_l]} u^{i,l} = \mathbf{1} \right\}. \quad (12)$$

The idea is that the vectors u encode the activation decisions of all neurons, i.e. $u_j^{i,l} = 1$ if the outcome of the j -th component of layer l lies in the interval $[\underline{\beta}^{i,l}, \bar{\beta}^{i,l})$ and 0 otherwise. The constraint $\sum_{i \in [k_l]} u^{i,l} = \mathbf{1}$ ensures that for each neuron exactly one interval is chosen. We call a vector $u \in \mathcal{A}$ an *activation pattern*.

We can now prove the following theorem which shows that the uncertainty set $U_f(W, \bar{c}, R)$ is given by a finite union of convex sets, where each convex set is an intersection of a polyhedron with a norm constraint. To this end, we define $\tilde{W}^1 = W^1$, $W^{L+1} = \text{Id}$, and

$$\tilde{W}^l = \left(\prod_{s=1}^{l-1} W^{s+1} \text{diag} \left(\sum_{i \in [k_s]} u^{i,s} \alpha_i^s \right) \right) W^1$$

for each $l = 2, \dots, L+1$. Furthermore, we set $\tilde{\gamma}^1 = 0$ and

$$\tilde{\gamma}^l = \sum_{s=2}^l W^l \left(\prod_{t=s}^{l-1} \text{diag} \left(\sum_{i \in [k_t]} u^{i,t} \alpha_i^t \right) W^t \right) \left(\sum_{i \in [k_{s-1}]} u^{i,s-1} \gamma_i^{s-1} \right)$$

for all $l = 2, \dots, L + 1$.

Theorem 1. *Given the weight matrices W of a trained neural network, a center point $\bar{c} \in \mathbb{R}^{d_L}$ and a radius $R > 0$, then it holds that*

$$U_f(W, \bar{c}, R) = \bigcup_{u \in \mathcal{A}} P(W, u, \bar{c}, R) \quad (13)$$

with

$$\begin{aligned} P(W, u, \bar{c}, R) := \{c \in \mathbb{R}^N : & \tilde{W}^l c + \tilde{\gamma}^l < \sum_{i \in [k_l]} u^{i,l} \bar{\beta}^{i,l} \quad \forall l \in [L], \\ & \tilde{W}^l c + \tilde{\gamma}^l \geq \sum_{i \in [k_l]} u^{i,l} \underline{\beta}^{i,l} \quad \forall l \in [L], \\ & \|\tilde{W}^{L+1} c + \tilde{\gamma}^{L+1} - \bar{c}\| \leq R\}. \end{aligned}$$

Proof. It is a well-known fact that neural networks with classical piecewise affine activation functions cluster the data space into polyhedra and apply an different affine function on each of them [RR17, MPCB14, WBB18, RPK⁺17]. Nevertheless we will derive our result explicite for the more general piecewise affine activation functions in this proof.

Note that for each data point $c \in \mathbb{R}^N$ applied to the neural network, there exists exactly one activation pattern $u \in \mathcal{A}$. Consider a fixed activation pattern $u \in \mathcal{A}$, and for a data point $c \in U_f(W, \bar{c}, R)$ let $\tilde{w}^l(c) \in \mathbb{R}^{d_l}$ be the output of layer $l \in [L]$ before applying the activation function. The data point c has activation pattern u if the conditions

$$\sum_{i \in [k_l]} u^{i,l} \underline{\beta}^{i,l} \leq \tilde{w}^l(c) < \sum_{i \in [k_l]} u^{i,l} \bar{\beta}^{i,l} \quad (14)$$

are true for each $l \in [L]$. The output of layer 1 is given by $W^1 c$. Applying the activation function componentwise and afterwards applying W^2 , the output of layer 2 is given by

$$\begin{aligned} \tilde{w}^2 &= W^2 \left(\text{diag} \left(\sum_{i \in [k_1]} u^{i,1} \alpha_i^1 \right) W^1 c + \left(\sum_{i \in [k_1]} u^{i,1} \gamma_i^1 \right) \right) \\ &= W^2 \text{diag} \left(\sum_{i \in [k_1]} u^{i,1} \alpha_i^1 \right) W^1 c + W^2 \left(\sum_{i \in [k_1]} u^{i,1} \gamma_i^1 \right) \\ &= \tilde{W}^2 c + \tilde{\gamma}^2. \end{aligned}$$

Inductively we conclude that the output of layer $l \in [L]$ is $\tilde{W}^l c + \tilde{\gamma}^l$ and together with (14) we obtain the linear inequalities in $P(W, u, \bar{c}, R)$. Since the activation function is applied to the output of the last layer, applying the identity matrix W^{L+1} afterwards we obtain the output of the neural network by

$$f_{W^1, \dots, W^L}(c) = \tilde{W}^{L+1} c + \tilde{\gamma}^{L+1}.$$

Since for any data point in $U_f(W, \bar{c}, R)$ the condition $\|f_{W^1, \dots, W^L}(c) - \bar{c}\| \leq R$ must hold, we obtain the last constraint in the set $P(W, u, \bar{c}, R)$ which proves the result. \square

Note that the set $P(W, u, \bar{c}, R)$ can be unbounded since if there exists a point $\hat{c} \in P(W, u, \bar{c}, R)$, the polyhedron corresponding to the linear constraints has an infinite ray $r \in \mathbb{R}^N$ and if r is in the kernel of the matrix \tilde{W}^{L+1} then each point $\hat{c} + \lambda r$ for $\lambda \in [0, \infty)$ is contained in $P(W, u, \bar{c}, R)$.

Estimating the size of \mathcal{A} , we find the following result.

Corollary 2. *The uncertainty set $U_f(W, \bar{c}, R)$ is the union of at most $(d(k-1))^{NL}$ convex sets $P(W, u, \bar{c}, R)$, where $k = \max_{l \in [L]} k_l$ and $d := \max_{l \in [L]} d_l$.*

Proof. The idea of the proof is to bound the number of possible regions which arise by the linear inequalities in the definition of $P(W, u, \bar{c}, R)$. It was proved in [RPK⁺17] that given t hyperplanes in \mathbb{R}^N , the number of regions (i.e. the number of connected open sets bounded on some sides by hyperplanes) is bounded from above by t^N . Considering the linear inequalities in $P(W, u, \bar{c}, R)$, in the first layer we have at most $d(k-1)$ hyperplanes describing the feasible region, since we have at most d normal vectors and for each at most $k-1$ intervals given by the right hand sides. Therefore, the number of regions is bounded by $(d(k-1))^N$. Considering one of the regions, it has fixed activation pattern for the first layer and is then again divided into at most $(d(k-1))^N$ regions by the hyperplanes of the second layer. Hence, after the second layer we have at most $(d(k-1))^{2N}$ possible regions. Inductively we conclude that the number of possible regions given by the constraints in $P(W, u, \bar{c}, R)$ is bounded by $(d(k-1))^{NL}$. \square

Note that if every layer has ReLU activation (which is continuous) and we choose the Euclidean norm, then

$$P(W, u, \bar{c}, R) := \{c \in \mathbb{R}^N \mid \begin{aligned} &\tilde{w}_j^l c \leq 0 \text{ if } u_j^{l,1} = 1 \text{ and } u_j^{l,2} = 0 \ \forall j \in [d_l], l \in [L], \\ &\tilde{w}_j^l c \geq 0 \text{ if } u_j^{l,1} = 0 \text{ and } u_j^{l,2} = 1 \ \forall j \in [d_l], l \in [L], \\ &c^\top (\tilde{W}^{L+1})^\top \tilde{W}^{L+1} c - 2c^\top \tilde{W}^{L+1} \bar{c} + \|\bar{c}\|^2 \leq R^2 \}. \end{aligned}$$

Therefore, applying Theorem 1 and Corollary 2 to the ReLU case, $U_f(W, \bar{c}, R)$ is the union of $\mathcal{O}(d^{NL})$ polyhedral cones intersected with the level set of one convex quadratic function.

A direct consequence of Theorem 1 is that in general the uncertainty set $U_f(W, \bar{c}, R)$ is not convex. Therefore, the robust optimization problem (2) cannot be reformulated using classical duality results. Nevertheless it is possible to optimize over $U_f(W, \bar{c}, R)$ in direction $x \in \mathbb{R}^N$ by solving for each $u \in \mathcal{A}$ the problem

$$\max_{c \in P(W, u, \bar{c}, R)} x^\top c$$

or deciding that it is infeasible. Then the best solution over all sets $P(W, u, \bar{c}, R)$ is the optimal solution. Alternatively it is possible to optimize over $U_f(W, \bar{c}, R)$ by solving a convex quadratic mixed-integer program. A similar idea was already used to model trained neural networks with ReLU activation in [FJ18] and to train binarized neural networks in [IIC⁺19, BK20].

Theorem 3. *For a given solution $x \in X$ and a continuous activation function, the problem*

$$\max_{c \in U_f(W, \bar{c}, R)} c^\top x$$

is equivalent to the problem

$$\max x^\top c^1 \tag{15}$$

$$s.t. \quad W^l c^l < \sum_{i \in [k_l]} u^{i,l} \bar{\beta}^{i,l} \quad \forall l \in [L] \tag{16}$$

$$W^l c^l \geq \sum_{i \in [k_l]} u^{i,l} \underline{\beta}^{i,l} \quad \forall l \in [L] \tag{17}$$

$$c^{l+1} = \text{diag}\left(\sum_{i \in [k_l]} u^{i,l} \alpha_i^l\right) W^l c^l + \sum_{i \in [k_l]} u^{i,l} \gamma_i^l \quad \forall l \in [L] \tag{18}$$

$$\sum_{i \in [k_l]} u^{i,l} = \mathbf{1} \quad \forall l \in [L] \tag{19}$$

$$\|c^{L+1} - \bar{c}\| \leq R \tag{20}$$

$$u^{i,l} \in \{0, 1\}^{d_i} \quad \forall i \in [k_l], l \in [L] \tag{21}$$

$$c^l \in \mathbb{R}^{d_l} \quad \forall l \in [L+1]. \tag{22}$$

Proof. The set of feasible variable assignments of the variables $u^{i,l}$ are exactly all possible activation patterns in \mathcal{A} . The constraints (16)-(17) ensure that the activation pattern given by the u -variables is true for the data point $c^1 \in \mathbb{R}^N$. Furthermore, the variables c^{l+1} model the output of layer l after applying the activation function componentwise. Following the proof of Theorem 1, the set of feasible solutions $c^1 \in \mathbb{R}^N$ of the formulation is equal to $U_f(W, \bar{c}, R)$. \square

Note that the quadratic terms in Constraint (18) can be linearized by standard linearization techniques. Therefore, the problem in Theorem 3 is equivalent to a mixed-integer program with a convex quadratic constraint if we use the Euclidean norm, or a mixed-integer linear program if we use the ℓ_1 -norm. Hence, the adversarial Problem (4) can be solved by this formulation using classical integer programming solvers as CPLEX or Gurobi. Using the iterative constraint generation procedure (see Section 2), we can then solve the robust problem (2).

We conclude this section by describing an alternative solution method to simplify the adversarial problem (15-22) by avoiding the use of binary variables $u^{i,l}$. To this end, we apply all scenarios c^1, \dots, c^m from the training data to the neural network to calculate the activation pattern for each of them, i.e. calculating the values of the u -variables for each data point c^j which we denote by $u^{i,l}(c^j)$ for all $i \in [k_l], l \in [L], j \in [m]$. These values correspond to those sets $P(W, u, \bar{c}, R)$ that contain actual training data. Having determined $S := \{u(c^1), \dots, u(c^m)\} \subset \mathcal{A}$, we then solve (15-22) repeatedly for each choice of $u \in S$. This means that we solve possibly up to m problems (in practice, $|S| \ll m$), where each problem is given as a quadratic convex program which can be solved efficiently. Furthermore, solving these problems can be easily parallelized. This approach to generating adversarial scenarios is used in the following experiments.

4 Experiments

In the following we conduct three experiments to assess the quality of the robust solutions found by our approach based on constructing uncertainty sets via deep neural networks (denoted as NN in the following). To this end, we compare against the current state of the art, which is to construct polyhedra based on support vector clustering with suitable kernel (denoted as Kernel), see Section 2.

The first experiment considers low-dimensional data to give an intuitive description of the differences between the two approaches. We then conduct higher-dimensional tests on randomly

generated data to gain statistical insights. Finally, we conduct an experiment with real traffic-data from the City of Chicago.

All experiments were carried out on a virtual machine running Ubuntu 18.04. and using eight Intel Xeon CPU E7-2850 processors. Code was implemented in Python, where we solved mathematical programs with Gurobi version 9.0.3 (except for solving the Kernel training problem (7), where CPLEX version 12.8 was used). To train neural networks, we used the PyTorch implementation from [RVG⁺18], which is available online¹. When training neural networks, we repeat the process three times and use the network that gives the best loss value. Our code and data is made available online² as well.

4.1 Experiment 1: Illustrative Examples

The purpose of this experiment is to derive an intuitive understanding of the differences between our approach and the kernel-based approach. To this end we generate two-dimensional data and use it as scenarios for a simple two-dimensional optimization problem.

To generate data sets, we use [SHY17] as a starting point. There are three types of data we consider. The first type is bivariate normal distributed (denoted as *Gaussian*), where we create random positive definite covariance matrices using the sklearn package. The second type consists of two such distributions that are created independently; for each data point that is sampled, we decide with equal probability whether the first or the second distribution is used (denoted as *Mixed Gaussian*). Finally, the third set is sampled uniformly from a polyhedron that is constructed in the manner of budgeted uncertainty [BS04]. That is, scenarios are sampled from sets

$$\mathcal{U} = \{c : c_i = \underline{c}_i + \bar{c}_i \delta_i, \sum_{i=1}^n \delta_i \leq \Gamma\}$$

where the lower and upper bounds \underline{c}_i and \bar{c}_i are chosen randomly and $n = 2$, $\Gamma = 1$ (denoted as *Polyhedral*).

We sample 475 points for training and 10,000 data points for testing in each set. Additionally, for each training set we uniformly sample 25 points in $[0, 300]^n$ to simulate outliers, which means in total the training sets contain 500 points where 5% are outliers.

For NN, we use neural networks with three layers of dimensions 2×15 , 15×15 and 15×15 , respectively, with a ReLU operator after the first and second layer. To train the networks, we use a loss function that aims at minimizing the radius of data points preceding the 90% radius quantile, and maximizing the radius of subsequent data points. To calculate the loss function, we sort the radii of the 500 points. Let $r_{\pi(1)} \leq r_{\pi(2)} \leq \dots \leq r_{\pi(500)}$ be such a sorting. The loss is then calculated as $\sum_{i=1}^5 5i \cdot r_{\pi(450-i)} - \sum_{i=1}^5 i \cdot r_{\pi(450+i)}$. This way, we enforce the network to include those data points where the classification confidence is high, and to exclude the others. After training, we use a radius quantile of 90% for our uncertainty set $U_f(W, \bar{c}, R)$. For Kernel, we use $\nu = 0.1$, corresponding to a 90% quantile as well.

In Figure 1 we show representative examples for each data set. White crosses indicate the training data points. The first two figures show the Gaussian set, the middle two figures show the Mixed Gaussian set, and the last two figures show the Polyhedral set.

Figures on the left show the radius the neural network associates with each point, where a white line shows the level set of the 90% radius quantile; i.e., all points within the white lines are considered as possible scenarios. For the figures on the right, we show the value $\sum_{i \in \text{SV}} \alpha_i v_i^\top \mathbf{1}$

¹<https://github.com/lukasruff/Deep-SVDD-PyTorch>

²<http://robust-optimization.com/data/deeplearningpaper/data.zip>

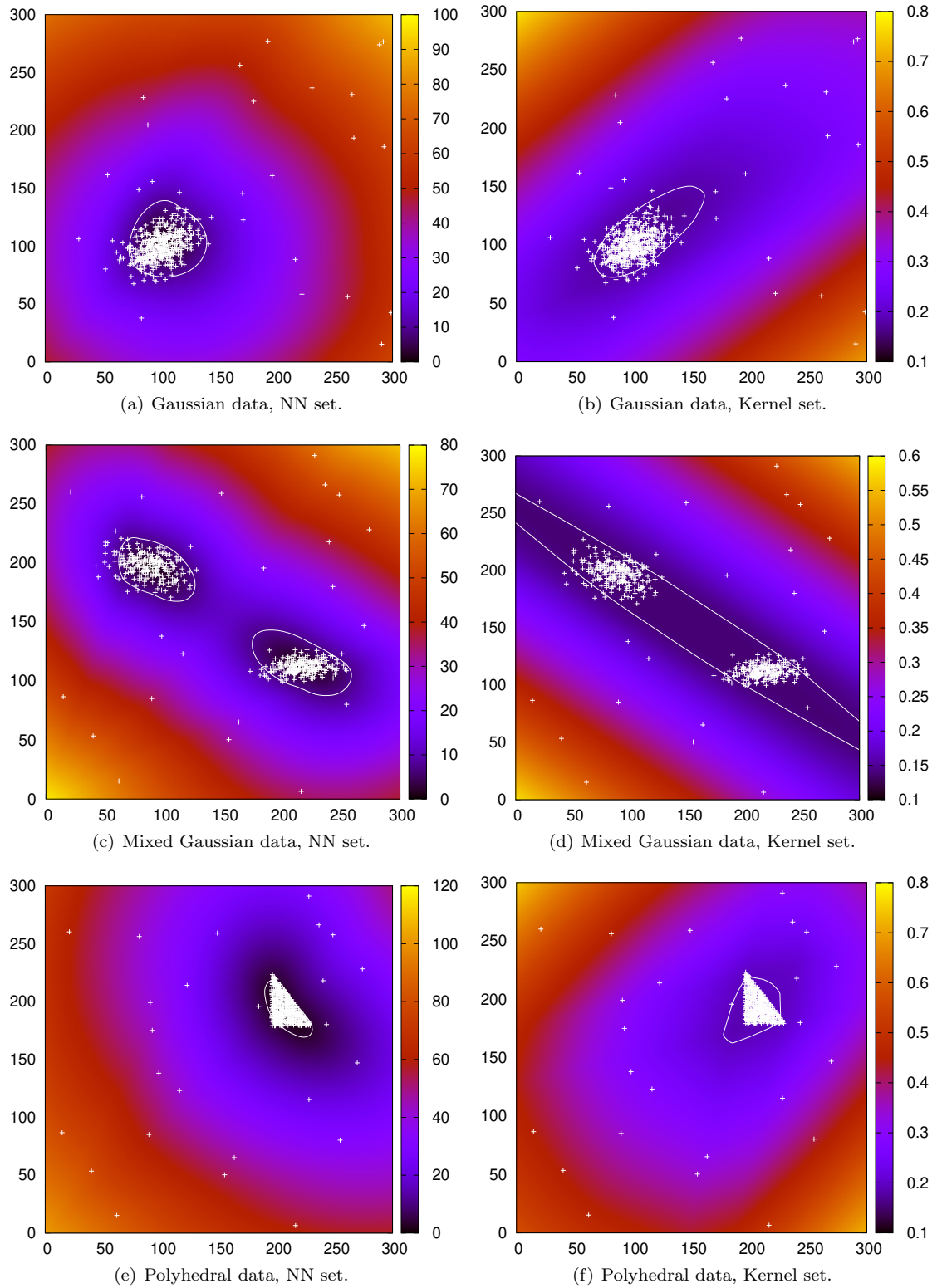


Figure 1: Visual comparison of uncertainty sets in experiment 1.

with $v_{ij} = |(Q(c - c^i))_j|$. The white line indicates those points where this value is less or equal to $\min_{i' \in \text{BSV}} \sum_{i \in \text{SV}} \alpha_i \|Q(c^{i'} - c^i)\|_1$, i.e., points that are considered as possible scenarios by Kernel.

Comparing these plots, we first note that both NN and Kernel can reasonably identify the core region of relevant scenarios against which to protect. For the Gaussian data, both uncertainty sets are similar, with the Kernel set being slightly more elongated towards the top right, where some of the outliers are situated. The difference between NN and Kernel is more pronounced for Mixed Gaussian data. It can be seen that the uncertainty set produced by Kernel is a convex polyhedron, which means that the two data clusters do not become separated. This results in a long and thin uncertainty set. Using NN, it is possible to create non-convex, non-connected uncertainty sets, which reflects the original data well. Finally, for Polyhedral data, both approaches can again identify the rough position of data, separating from the noise. The Kernel set shows an elongation towards the noise, while NN remains more compact.

To summarize Figure 1, we find that NN is able to fit uncertainty sets in these examples that are visually more suitable to represent the uncertainty than it is the case when using Kernel. However, this does not necessarily translate to a better performance of robust solutions. To test this, we use the uncertainty sets from Figure 1 to solve two types of optimization problems. In the first type, the uncertainty is in the objective. We use a simple budget constraint in addition, which results in optimization problems of the form

$$\begin{aligned} \min \quad & \max_{(c_1, c_2) \in U} c_1 x_1 + c_2 x_2 & (\text{Obj}) \\ \text{s.t.} \quad & x_1 + x_2 = 0.3 \\ & x_1, x_2 \in [-1, 1]. \end{aligned}$$

In the second type of problems, we assume that the uncertainty is in the constraints, and solve

$$\begin{aligned} \max \quad & x_1 + x_2 & (\text{Feas}) \\ \text{s.t.} \quad & c_1 x_1 + c_2 x_2 \leq 0 \quad \forall (c_1, c_2) \in U \\ & x_1, x_2 \in [-1, 1], \end{aligned}$$

where in both cases U can be replaced by the uncertainty set generated by Kernel or by NN.

In Figures 2 and 3 we present an evaluation of the optimal solutions for NN and Kernel uncertainty sets. For plots in Figure 2, we solved problem (Obj) using the 90% confidence sets depicted in Figure 1. This means that for each of the three data sets and each of the two uncertainty sets, we find one solution. This solution is then evaluated out-of-sample (i.e. on the test set), resulting in a histogram that shows the objective value performance. The solid vertical line indicates the 90% quantile of the out-of-sample objective values, while the dashed vertical line shows the mean value.

Interestingly, a visually better fitted uncertainty set does not always result in robust solutions that perform better. For both the Gaussian and the Mixed Gaussian data, both solutions are equally good. For the Polyhedral data, NN shows slightly better performance at the 90% quantile, but at the cost of a worse performance on average. To understand this effect, we remark on two properties. First, in linear min-max optimization problems, solving with respect to some uncertainty set is equivalent to solving with respect to the convex hull of this set. This means that a non-convex set does not have an advantage in this setting (which can be different for robust two-stage problems). Second, with uncertainty in the objective function, scaling the uncertainty set has no impact on the out-of-sample quality of the solution. Multiplying all possible scenarios in the set with some scaling factor $\lambda > 0$ results in the same optimal solution. Hence, only the shape and position of the uncertainty set is of relevance, which is counter-intuitive when assessing the quality of uncertainty sets visually.

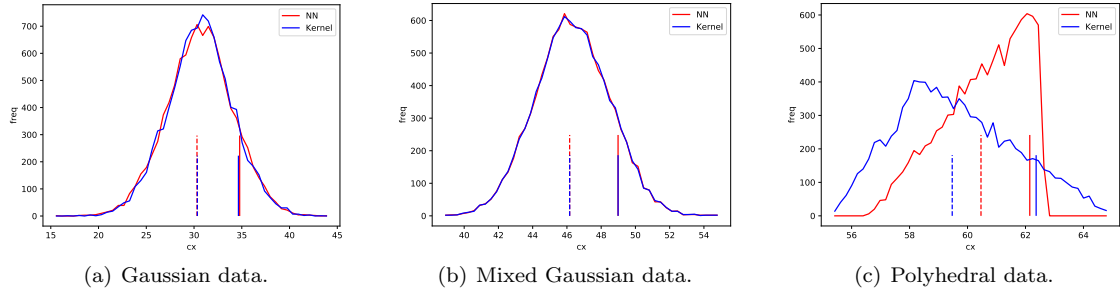


Figure 2: Objective values in experiment 1.

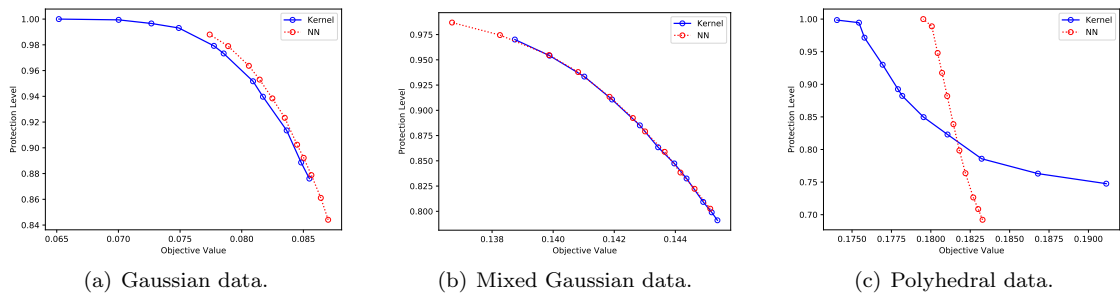


Figure 3: Feasibility vs objective values in experiment 1.

We now consider plots in Figure 3, where we compare feasibility against objective value. Here we use different protection levels, ranging from 40% to 90%, to solve Problem (Feas). Note that NN only needs to be trained once, and we can adjust the protection level by using different quantile values for the radius R . For Kernel, we recompute the polyhedron with every desired protection level, adjusted by the parameter ν . In Figure 3 we show the resulting objective value on the horizontal axis, and the protection level on the vertical axis, that is, we determine how often a solution is feasible with respect to the out-of-sample data. Good solutions are in the top right corner, having both a large objective value and a high degree of robustness.

Similar to what could be observed when solving problem (Obj), the results are mixed. For Gaussian data, there is a slight advantage for NN, where solutions that give the same objective value as Kernel solutions result in higher feasibility. For Mixed Gaussian data, the curves overlap. For Polyhedral data, we see that NN solutions have a better performance when considering large quantiles (i.e. high feasibility with smaller objective values), but the performance becomes worse than that of Kernel solutions for smaller quantiles (i.e., smaller feasibility with higher objective value).

The results presented in this section are illustrative insofar they only use two-dimensional data and only one random data set per instance type. We analyze the statistical performance of solutions in the next experiment.

4.2 Experiment 2: Random Data Experiments

In this experiment, we measure the performance of NN and Kernel solutions on 20-dimensional, randomly generated data. The setup is similar to that of the first experiment. Data is generated in the same manner, where $n = 20$ and $\Gamma = n/2 = 10$. For each type of data (Gaussian, Mixed Gaussian, Polyhedral), we generate 10 instances. For Mixed Gaussian data, we additionally ensure that the mean-points of the two distributions do not lie in the same quadrant.

For each instance, the neural network is trained with three layers of dimensions 20×50 , 50×50 and 50×50 , with a ReLU operator after the first and second layer. Using uncertainty sets generated this way, we solve 20-dimensional variants of Problem (Obj) with a right-hand side value of 10 and Problem (Feas).

Type	Avg		90% Quantile	
	NN	Kernel	NN	Kernel
Gaussian	1021.1	1409.5	1057.9	1440.1
Mixed Gaussian	1098.4	1413.4	1153.4	1445.7
Polyhedral	1093.1	1461.8	1154.1	1505.0

Table 1: Average objective values in experiment 2.

We first discuss results on problems of type (Obj). Table 1 shows the average of the average out-of-sample objective value and the average of the 90%-quantile out-of-sample objective value for both NN and Kernel. Recall that the aim is to minimize the objective value. We see that NN strongly outperforms Kernel on all three instance classes with respect to both average and quantile performance. In Section A in the appendix, we present additional results on each of the thirty test instances (see Table 2). Furthermore, Figure 4 shows a representative performance histogram for one instance of each class. It can be seen that, while both approaches showed similar performance on the two-dimensional examples, the NN scales much better with higher-dimensional data. At the same time, this comes with a cost: Solving one problem of type (Obj) takes on average 0.5 seconds with the compact Kernel formulation, but 174.3 seconds when using the iterative procedure required for solving problems with NN uncertainty.

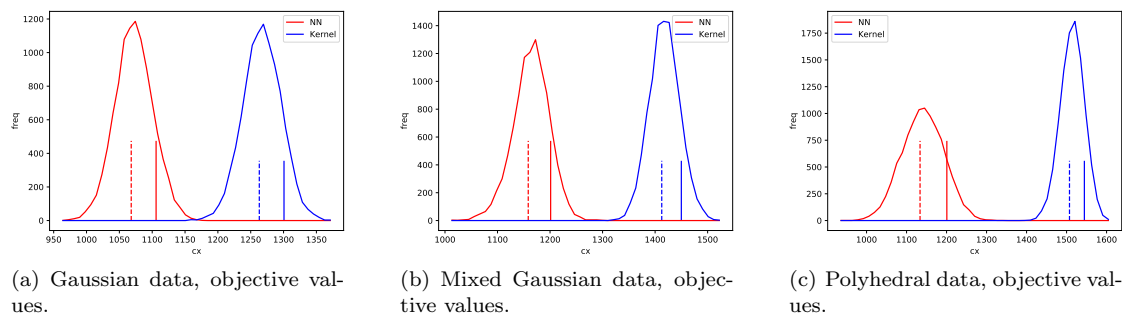


Figure 4: Example plots in experiment 2.

We now consider the performance when solving problems of type (Feas). In Figure 5, we show the average objective value versus feasibility curves for each instance class. While the curves represented a good trade-off between these two goals for the two-dimensional data, this is not always the case on high dimensional data, i.e., solutions are not always Pareto efficient. The

protection levels of both approaches is much higher than the quantile-values (ranging from 40% to 90%) that were used. This may indicate that the uncertainty sets are larger than required.

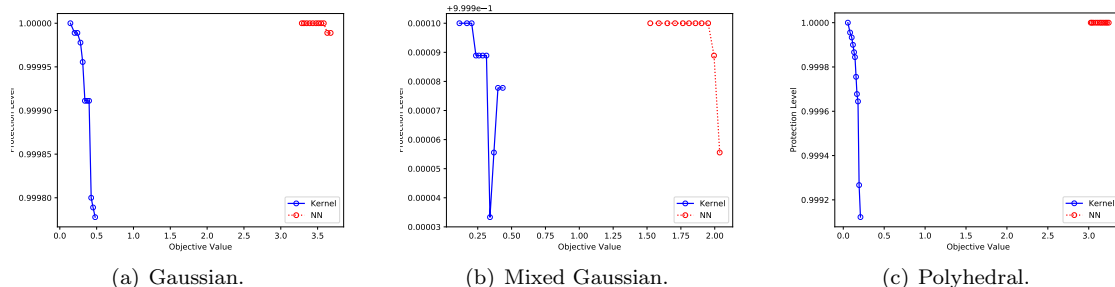


Figure 5: Average feasibility vs objective in experiment 2.

Comparing Kernel and NN solutions, again we find that NN shows a considerably better performance. NN solutions reach a consistently higher level of feasibility while also giving a larger profit. As Figure 5 shows average results, we also present the trade-off between feasibility and objective value for each instance in the appendix (Tables 3-5). In these tables, *Infeas* gives the absolute number of infeasible instances out of 10,000 out-of-sample instances that were used.

4.3 Experiment 3: Real-World Data Experiments

While the results of the second experiment demonstrate strong dominance of NN solutions over Kernel solutions, instances were randomly generated and are thus not necessarily representative for real-world data. For this reason as a third experiment we solve the shortest path problem with travel time uncertainty using the travel time data of the City of Chicago that was first collected and used in [CDG19]. Travel times for each arc in the Chicago network were collected from March to May 2017 through a live traffic data interface. The whole network has 1308 arcs and 538 nodes, but for this experiment, we only use the inner city region containing 189 arcs and 165 nodes. Furthermore, we use scenarios representing weekend travel times. There is a total of 1141 such observations (each observation giving the travel time for every arc in the network), of which we use 570 for training and 571 for testing.

While solving compact formulations with the Kernel approach was fast in the 20-dimensional case, here a drawback is revealed. The compact model has $O(n|SV|)$ variables, where SV is the set of support vectors defined in Section 2 whose size depends on the number of training samples and the protection level. Therefore, with a large number of scenarios, the problem can grow too large to be solvable (or even to be loaded into random access memory). For the NN approach, training data is only used to tune the neural network, and not during the robust optimization process itself. Due to the high efficiency of training algorithms as the stochastic gradient descent in this model, large data sets can be handled more easily. Due to this observation, we restricted the experiment to the city center graph and weekend scenarios (other, larger data sets were available as well). Furthermore, we used a 95% quantile instead of 90% as in the previous experiments, as this further reduces the size of the set SV .

Due to the way the graph is generated, there exist edges that are completely correlated. This happens as original travel speed observations were collected on segments that may contain multiple edges. As the covariance matrix becomes degenerate in this case, small random noise was added to the travel times to calculate the Kernel sets. Note that the covariance matrix is not

used in the training process of NN. The neural network we used has three layers of size 189×50 , 50×50 and 50×50 , respectively.

The robust optimization problem we consider here is to find a shortest path over the uncertain data where the uncertainty is only present in the objective function. We generate ten random source-sink pairs, where we ensure that at least eight arcs need to be traversed from source to sink to exclude pairs that are nearby. For each source-sink pair, a robust path is calculated using NN and Kernel. On average after training, Kernel paths take 1497.7 seconds to compute, while NN paths take 794.8 seconds.

We present results on this experiment in Figures 6-8. In each figure, we show the path computed by Kernel on the left and the path computed by NN on the right. In the middle, we show the out-of-sample histogram of travel times for these paths.

We note that classical flow constraints (for each node except source and sink, inflow equals outflow) correctly model the path problem only if all costs are non-negative. Using the Kernel approach, we observed that solutions frequently were not connected and included cycles, which results from uncertainty sets that include negative costs. We modified the Kernel approach such that only non-negative arc lengths are contained in the uncertainty set. In two instances (paths 05 and 09) it can be observed that there still exists a single edge that is traversed twice in an unnecessary loop. This can only happen if the Kernel approach assumes that such costs are equal to zero. Apart from these two instances, all paths (both Kernel and NN) seem reasonable options in the street network. Note that in no case we observe the same path from Kernel and NN.

Comparing the out-of-sample performance, there are five instances with mixed results (paths 01, 04, 06, 07, and 10). For these solutions histograms largely overlap and paths contain similar edges. In case of paths 01 and 10, Kernel shows better average and better 95% quantile performance. For paths 04, 06, and 07, this comparison gives NN the advantage. For the other five paths (02, 03, 05, 08, and 09), NN has a distinct advantage, clearly outperforming Kernel.

To summarize the findings of these three experiments, we note that (i) when visualized on low-dimensional data, NN uncertainty sets reasonably capture the shape and size of uncertainty; (ii) NN uncertainty sets on random, 20-dimensional optimization problems result in significantly better solutions than what Kernel achieves, irrespective whether we consider objective or constraint uncertainty, but at the cost of higher computational effort; and (iii) using real-world data, NN becomes more computationally efficient, scaling better in the problem size than Kernel, but still produces solutions that clearly outperform those produced by Kernel.

5 Conclusions

To derive useful robust optimization models, it is central to have a suitable description of the uncertainty set available. The task of identifying whether a given scenario is similar to observed data or should be considered as an outlier is related to the task of describing the uncertainty set, and is a typical problem for which machine learning techniques have been proven to be highly efficient.

In this paper we combined one-class deep neural networks, to describe the uncertainty set, with robust optimization models. It turns out that the uncertainty sets created by the one-class deep neural networks are a finite union of convex sets, each set being a polyhedron intersected with a convex norm-constraint. Therefore, our constructed sets may have a more complex structure than other data-driven sets. To solve the robust optimization problem, it is necessary that we can optimize over the set of scenarios that are classified as being representative for the historic data by the neural network. We show that this is possible by formulating the adversarial problem

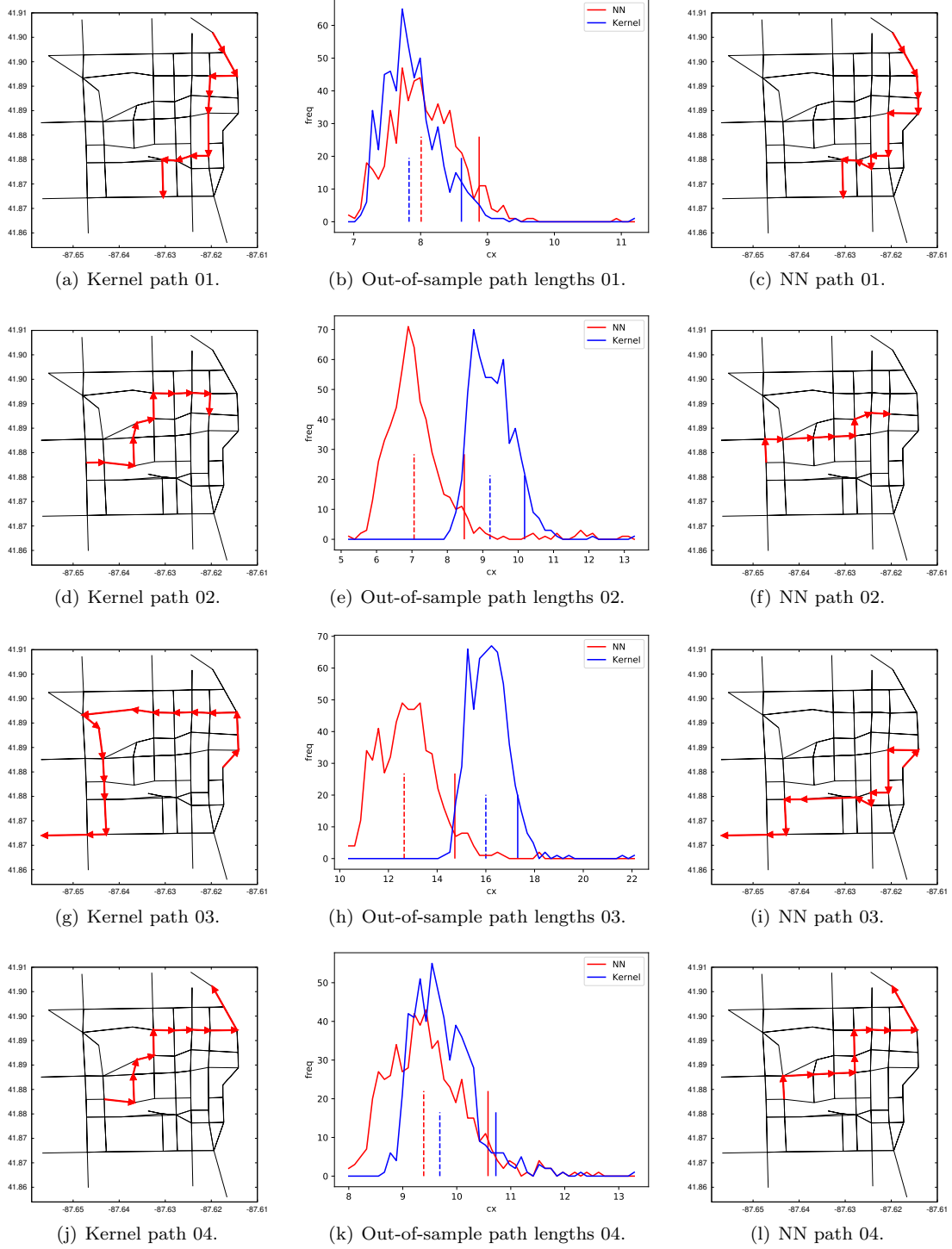


Figure 6: Comparison of paths 1-4 in experiment 3.

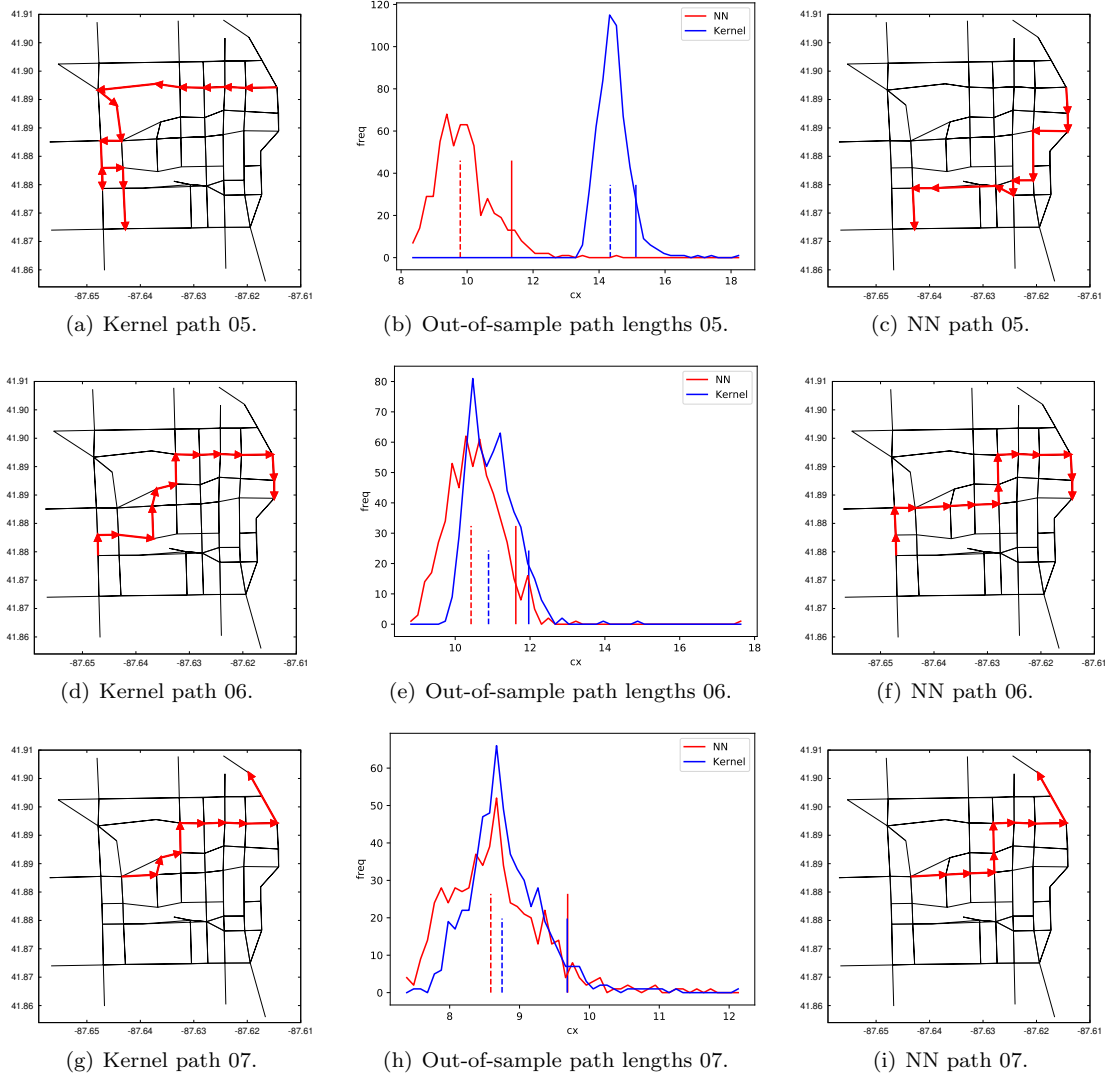


Figure 7: Comparison of paths 5-7 in experiment 3.

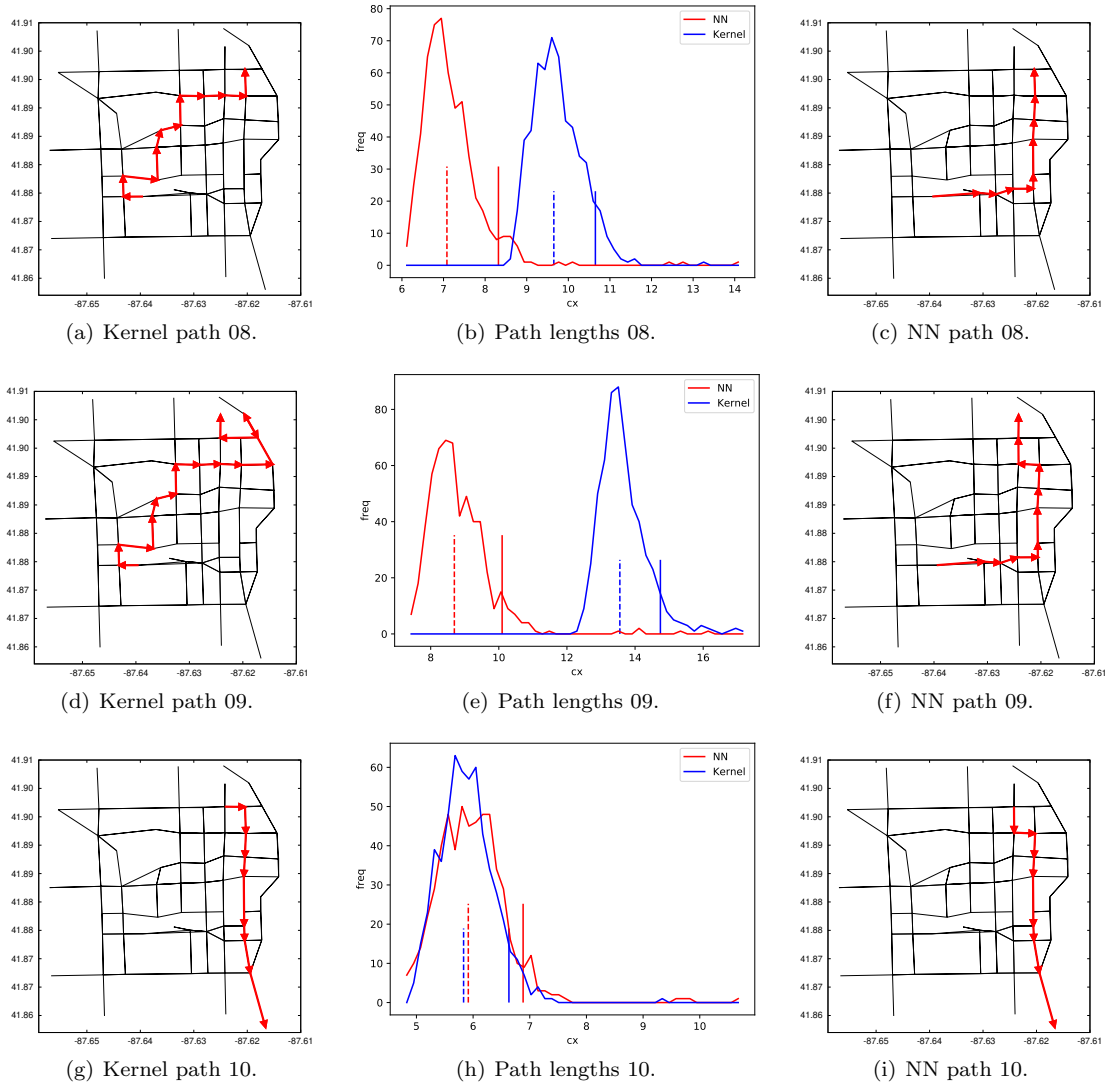


Figure 8: Comparison of paths 8-10 in experiment 3.

as a convex quadratic mixed-integer program. By further decomposing this problem using the historic data, it is even possible to remove the binary variables from the program.

We tested our method using three experiments, where we compare against a kernel-based support vector clustering method as a representative of the state-of-the-art that is most similar to our approach. Throughout our experiments, we found encouraging results, observing that the method proposed in this paper finds better robust solutions (with respect to both objective value and feasibility) than when applying the previous method. At the same time, our method is easy to apply with suitable training and optimization code being readily available, and scales well in the training data size.

Since in the classical linear robust optimization regime the uncertainty set can always be replaced by its convex hull, the non-convexity (and even non-connectedness) of our uncertainty set is implicitly reverted and does not have an impact on the performance. Considering two-stage robust optimization problems, replacing the uncertainty set by its convex hull is not possible anymore, and therefore extending our method to two-stage robust optimization problems in the future can lead to larger improvements compared to other uncertainty sets as the ones constructed by kernel-based SVC.

References

- [AB20] Polina Alexeenko and Eilyan Bitar. Nonparametric estimation of uncertainty sets for robust optimization. *arXiv preprint arXiv:2004.03069*, 2020.
- [ABV09] Hassene Aissi, Cristina Bazgan, and Daniel Vanderpooten. Min-max and min-max regret versions of combinatorial optimization problems: A survey. *European Journal of Operational Research*, 197(2):427–438, 2009.
- [BBV04] Stephen Boyd, Stephen P Boyd, and Lieven Vandenbergh. *Convex optimization*. Cambridge university press, 2004.
- [BGK18] Dimitris Bertsimas, Vishal Gupta, and Nathan Kallus. Data-driven robust optimization. *Mathematical Programming*, 167(2):235–292, 2018.
- [BK18] Christoph Buchheim and Jannis Kurtz. Robust combinatorial optimization under convex and discrete cost uncertainty. *EURO Journal on Computational Optimization*, 6(3):211–238, 2018.
- [BK20] Bubacarr Bah and Jannis Kurtz. An integer programming approach to deep neural networks with binary activation functions. *Workshop on Beyond first-order methods in ML systems at the 37th International Conference on Machine Learning, Vienna, Austria*, 2020.
- [BS03] Dimitris Bertsimas and Melvyn Sim. Robust discrete optimization and network flows. *Math. Program.*, 98(1-3):49–71, 2003.
- [BS04] Dimitris Bertsimas and Melvyn Sim. The price of robustness. *Operations Research*, 52(1):35–53, 2004.
- [BTEGN09] Aharon Ben-Tal, Laurent El Ghaoui, and Arkadi Nemirovski. *Robust optimization*, volume 28. Princeton University Press, 2009.
- [BTN98] Aharon Ben-Tal and Arkadi Nemirovski. Robust convex optimization. *Mathematics of Operations Research*, 23(4):769–805, 1998.

- [BTN99] Aharon Ben-Tal and Arkadi Nemirovski. Robust solutions of uncertain linear programs. *Operations Research Letters*, 25(1):1–13, 1999.
- [CDG19] André Chassein, Trivikram Dokka, and Marc Goerigk. Algorithms and uncertainty sets for data-driven robust shortest path problems. *European Journal of Operational Research*, 274(2):671–686, 2019.
- [CH15] Trevor Campbell and Jonathan P How. Bayesian nonparametric set construction for robust optimization. In *2015 American Control Conference (ACC)*, pages 4216–4221. IEEE, 2015.
- [DGR20] Trivikram Dokka, Marc Goerigk, and Rahul Roy. Mixed uncertainty sets for robust combinatorial optimization. *Optimization Letters*, 14(6):1323–1337, 2020.
- [EGL97] Laurent El Ghaoui and Hervé Lebret. Robust solutions to least-squares problems with uncertain data. *SIAM Journal on Matrix Analysis and Applications*, 18(4):1035–1064, 1997.
- [EGOL98] Laurent El Ghaoui, Francois Oustry, and Hervé Lebret. Robust solutions to uncertain semidefinite programs. *SIAM Journal on Optimization*, 9(1):33–52, 1998.
- [FJ18] Matteo Fischetti and Jason Jo. Deep neural networks and mixed integer linear optimization. *Constraints*, 23(3):296–309, 2018.
- [GGJ20] Francis Garuba, Marc Goerigk, and Peter Jacko. A comparison of data-driven uncertainty sets for robust network design. *arXiv preprint arXiv:2003.10507*, 2020.
- [HHL17] L Jeff Hong, Zhiyuan Huang, and Henry Lam. Learning-based robust optimization: Procedures and statistical guarantees. *arXiv preprint arXiv:1704.04342*, 2017.
- [IIC⁺19] Rodrigo Toro Icarte, León Illanes, Margarita P Castro, Andre A Cire, Sheila A McIlraith, and J Christopher Beck. Training binarized neural networks using MIP and CP. In *International Conference on Principles and Practice of Constraint Programming*, pages 401–417. Springer, 2019.
- [KY96] Panos Kouvelis and Gang Yu. *Robust Discrete Optimization and Its Applications*. Springer, 1996.
- [LDF11] Zukui Li, Ran Ding, and Christodoulos A Floudas. A comparative theoretical and computational study on robust counterpart optimization: I. robust linear optimization and robust mixed integer linear optimization. *Industrial & engineering chemistry research*, 50(18):10567–10603, 2011.
- [MPCB14] Guido F Montufar, Razvan Pascanu, Kyunghyun Cho, and Yoshua Bengio. On the number of linear regions of deep neural networks. In *Advances in neural information processing systems*, pages 2924–2932, 2014.
- [NY17] Chao Ning and Fengqi You. Data-driven adaptive nested robust optimization: general modeling framework and efficient computational algorithm for decision making under uncertainty. *AIChE Journal*, 63(9):3790–3817, 2017.
- [NY18] Chao Ning and Fengqi You. Data-driven decision making under uncertainty integrating robust optimization with principal component analysis and kernel smoothing methods. *Computers & Chemical Engineering*, 112:190–210, 2018.

- [PAS09] Bernardo K Pagnoncelli, Shabbir Ahmed, and Alexander Shapiro. Sample average approximation method for chance constrained programming: theory and applications. *Journal of optimization theory and applications*, 142(2):399–416, 2009.
- [RPK⁺17] Maithra Raghu, Ben Poole, Jon Kleinberg, Surya Ganguli, and Jascha Sohl-Dickstein. On the expressive power of deep neural networks. In *International conference on machine learning*, pages 2847–2854. PMLR, 2017.
- [RR17] Blaine Rister and Daniel L Rubin. Piecewise convexity of artificial neural networks. *Neural Networks*, 94:34–45, 2017.
- [RVG⁺18] Lukas Ruff, Robert Vandermeulen, Nico Goernitz, Lucas Deecke, Shoaib Ahmed Siddiqui, Alexander Binder, Emmanuel Müller, and Marius Kloft. Deep one-class classification. In *International conference on machine learning*, pages 4393–4402, 2018.
- [SHY17] Chao Shang, Xiaolin Huang, and Fengqi You. Data-driven robust optimization based on kernel learning. *Computers & Chemical Engineering*, 106:464–479, 2017.
- [Soy73] Allen L Soyster. Convex programming with set-inclusive constraints and applications to inexact linear programming. *Operations Research*, 21(5):1154–1157, 1973.
- [SY19] Chao Shang and Fengqi You. A data-driven robust optimization approach to scenario-based stochastic model predictive control. *Journal of Process Control*, 75:24–39, 2019.
- [TR14] Theja Tulabandhula and Cynthia Rudin. Robust optimization using machine learning for uncertainty sets. *arXiv preprint arXiv:1407.1097*, 2014.
- [WBB18] Zichao Wang, Randall Balestriero, and Richard Baraniuk. A max-affine spline perspective of recurrent neural networks. In *International Conference on Learning Representations*, 2018.
- [ZYX⁺08] Zhi-Qiang Zeng, Hong-Bin Yu, Hua-Rong Xu, Yan-Qi Xie, and Ji Gao. Fast training support vector machines using parallel sequential minimal optimization. In *2008 3rd international conference on intelligent system and knowledge engineering*, volume 1, pages 997–1001. IEEE, 2008.

A Additional Results of Experiment 2

Type	Inst.	Avg		Quantile	
		NN	Kernel	NN	Kernel
Gaussian	1	612.8	1329.2	651.7	1360.8
	2	1058.2	1444.2	1087.7	1477.5
	3	1273.7	1409.2	1309.7	1443.0
	4	1091.5	1437.8	1127.6	1469.1
	5	933.8	1461.4	964.0	1484.3
	6	1143.6	1432.0	1179.7	1463.8
	7	745.3	1411.5	787.5	1446.4
	8	1068.1	1263.1	1105.9	1300.7
	9	1430.5	1485.4	1464.4	1511.4
	10	853.1	1421.2	901.4	1444.1
Mixed Gaussian	1	1344.7	1466.0	1400.6	1502.4
	2	1147.5	1447.1	1206.7	1478.9
	3	1086.2	1423.1	1139.0	1452.0
	4	1158.5	1412.6	1201.1	1449.9
	5	1125.7	1446.0	1199.9	1473.8
	6	1010.8	1378.5	1066.2	1413.7
	7	957.4	1414.7	1003.2	1446.6
	8	856.5	1309.6	936.7	1346.3
	9	1076.1	1422.9	1121.6	1453.5
	10	1220.8	1413.8	1258.9	1440.4
Polyhedral	1	979.2	1497.1	1038.1	1545.0
	2	882.0	1434.8	942.3	1485.6
	3	1265.7	1406.4	1319.8	1454.0
	4	1083.8	1503.3	1151.3	1544.2
	5	1072.9	1479.2	1129.4	1515.3
	6	1055.9	1468.6	1111.3	1501.4
	7	1133.7	1507.3	1200.7	1544.5
	8	1259.4	1464.4	1314.5	1504.3
	9	1003.9	1467.2	1075.2	1511.1
	10	1194.3	1389.9	1258.7	1444.3

Table 2: Objective values in experiment 2.

Inst.			Quantile										
			0.40	0.45	0.50	0.55	0.60	0.65	0.70	0.75	0.80	0.85	0.90
1	Obj	NN	3.13	3.10	3.06	3.03	2.99	2.95	2.93	2.89	2.85	2.82	2.82
		Kernel	0.36	0.34	0.32	0.30	0.28	0.25	0.23	0.20	0.17	0.12	0.07
	Infeas	NN	0	0	0	0	0	0	0	0	0	0	0
		Kernel	1	1	0	0	0	0	0	0	0	0	0
2	Obj	NN	3.99	3.94	3.91	3.88	3.82	3.77	3.71	3.67	3.61	3.56	3.50
		Kernel	0.27	0.25	0.24	0.22	0.20	0.19	0.16	0.14	0.12	0.09	0.04
	Infeas	NN	19	18	17	8	8	8	4	2	1	1	0
		Kernel	0	0	0	0	0	0	0	0	0	0	0
3	Obj	NN	2.79	2.71	2.67	2.65	2.63	2.61	2.59	2.56	2.52	2.50	2.47
		Kernel	0.37	0.34	0.31	0.29	0.28	0.25	0.22	0.19	0.16	0.12	0.05
	Infeas	NN	0	0	0	0	0	0	0	0	0	0	0
		Kernel	0	0	0	0	0	0	0	0	0	0	0
4	Obj	NN	3.65	3.62	3.58	3.56	3.50	3.47	3.43	3.40	3.37	3.32	3.27
		Kernel	0.56	0.53	0.50	0.48	0.46	0.44	0.42	0.40	0.36	0.33	0.30
	Infeas	NN	0	0	0	0	0	0	0	0	0	0	0
		Kernel	0	0	0	0	0	0	0	0	0	0	0
5	Obj	NN	4.42	4.40	4.36	4.26	4.23	4.20	4.13	4.08	4.02	3.99	3.97
		Kernel	0.29	0.26	0.23	0.20	0.17	0.14	0.12	0.10	0.08	0.05	0.03
	Infeas	NN	0	0	0	0	0	0	0	0	0	0	0
		Kernel	0	0	0	0	0	0	0	0	0	0	0
6	Obj	NN	3.67	3.60	3.56	3.53	3.49	3.44	3.39	3.34	3.29	3.25	3.22
		Kernel	0.73	0.69	0.65	0.60	0.56	0.49	0.43	0.38	0.28	0.20	0.12
	Infeas	NN	0	0	0	0	0	0	0	0	0	0	0
		Kernel	0	0	0	0	0	0	0	0	0	0	0
7	Obj	NN	4.94	4.85	4.70	4.67	4.64	4.62	4.58	4.49	4.45	4.40	4.37
		Kernel	0.32	0.30	0.29	0.27	0.25	0.23	0.21	0.18	0.16	0.13	0.09
	Infeas	NN	1	1	1	0	0	0	0	0	0	0	0
		Kernel	0	0	0	0	0	0	0	0	0	0	0
8	Obj	NN	3.94	3.92	3.87	3.85	3.84	3.79	3.75	3.73	3.69	3.65	3.62
		Kernel	1.02	0.98	0.95	0.92	0.87	0.83	0.79	0.73	0.66	0.62	0.52
	Infeas	NN	0	0	0	0	0	0	0	0	0	0	0
		Kernel	0	0	0	0	0	0	0	0	0	0	0
9	Obj	NN	2.56	2.54	2.53	2.51	2.48	2.45	2.41	2.40	2.36	2.33	2.32
		Kernel	0.40	0.36	0.34	0.30	0.28	0.26	0.23	0.20	0.16	0.13	0.07
	Infeas	NN	0	0	0	0	0	0	0	0	0	0	0
		Kernel	0	0	0	0	0	0	0	0	0	0	0
10	Obj	NN	4.44	4.40	4.36	4.32	4.26	4.18	4.08	4.03	3.93	3.88	3.68
		Kernel	0.15	0.13	0.11	0.08	0.06	0.04	0.03	0.02	0.00	0.00	0.00
	Infeas	NN	0	0	0	0	0	0	0	0	0	0	0
		Kernel	0	0	0	0	0	0	0	0	0	0	0

Table 3: Feasibility vs objective on Gaussian data in experiment 2.

Inst.			Quantile										
			0.40	0.45	0.50	0.55	0.60	0.65	0.70	0.75	0.80	0.85	0.90
1	Obj	NN	1.90	1.89	1.87	1.85	1.83	1.80	1.76	1.71	1.67	1.65	1.62
		Kernel	0.76	0.73	0.71	0.67	0.65	0.61	0.57	0.53	0.50	0.41	0.27
	Infeas	NN	0	0	0	0	0	0	0	0	0	0	0
		Kernel	0	0	0	0	0	0	0	0	0	0	0
2	Obj	NN	1.70	1.69	1.67	1.66	1.64	1.61	1.59	1.57	1.55	1.54	1.51
		Kernel	0.57	0.53	0.49	0.46	0.43	0.40	0.37	0.35	0.31	0.28	0.21
	Infeas	NN	0	0	0	0	0	0	0	0	0	0	0
		Kernel	0	0	0	0	0	0	0	0	0	0	0
3	Obj	NN	1.76	1.70	1.68	1.65	1.63	1.60	1.52	1.50	1.47	1.44	1.40
		Kernel	0.09	0.06	0.04	0.00	0.00	0.00	0.00	0.00	0.00	0.00	0.00
	Infeas	NN	0	0	2	5	0	0	0	0	0	0	0
		Kernel	0	0	0	0	0	0	0	0	0	0	0
4	Obj	NN	2.27	2.24	2.18	2.10	2.05	2.02	1.98	1.93	1.85	1.80	1.74
		Kernel	0.47	0.43	0.40	0.37	0.33	0.31	0.29	0.27	0.24	0.21	0.13
	Infeas	NN	0	0	0	0	0	0	0	0	0	0	0
		Kernel	0	0	0	0	0	0	0	0	0	0	0
5	Obj	NN	1.95	1.92	1.86	1.83	1.79	1.76	1.71	1.63	1.58	1.35	1.31
		Kernel	0.25	0.22	0.19	0.15	0.11	0.10	0.07	0.05	0.03	0.00	0.00
	Infeas	NN	0	0	0	0	0	0	0	0	0	0	0
		Kernel	0	0	0	0	0	0	0	0	0	0	0
6	Obj	NN	2.11	2.10	2.06	1.98	1.93	1.90	1.86	1.83	1.77	1.74	1.69
		Kernel	0.68	0.64	0.60	0.57	0.53	0.48	0.42	0.39	0.34	0.28	0.18
	Infeas	NN	0	0	0	0	0	0	0	0	0	0	0
		Kernel	0	0	0	0	0	0	0	0	0	0	0
7	Obj	NN	2.02	1.99	1.95	1.91	1.81	1.75	1.71	1.64	1.55	1.49	1.43
		Kernel	0.32	0.30	0.28	0.25	0.23	0.21	0.18	0.16	0.13	0.11	0.06
	Infeas	NN	2	2	2	1	1	1	1	1	0	0	0
		Kernel	0	0	0	0	0	0	0	0	0	0	0
8	Obj	NN	2.68	2.59	2.54	2.43	2.35	2.22	2.17	2.09	2.03	2.01	2.00
		Kernel	0.66	0.62	0.59	0.58	0.56	0.52	0.50	0.49	0.46	0.42	0.36
	Infeas	NN	0	0	0	0	0	0	0	0	0	0	0
		Kernel	2	0	0	0	0	0	0	0	0	0	0
9	Obj	NN	1.91	1.83	1.80	1.77	1.74	1.70	1.66	1.55	1.49	1.40	1.35
		Kernel	0.36	0.34	0.31	0.28	0.25	0.22	0.19	0.15	0.11	0.07	0.02
	Infeas	NN	0	0	0	0	0	0	0	0	0	0	0
		Kernel	2	1	0	0	0	0	0	0	0	0	0
10	Obj	NN	1.92	1.88	1.83	1.79	1.76	1.72	1.67	1.63	1.56	1.51	1.28
		Kernel	0.51	0.46	0.44	0.41	0.37	0.34	0.29	0.27	0.22	0.16	0.08
	Infeas	NN	0	0	0	0	0	0	0	0	0	0	0
		Kernel	0	0	0	0	0	0	0	0	0	0	0

Table 4: Feasibility vs objective on Mixed Gaussian data in experiment 2.

Inst.			Quantile										
			0.40	0.45	0.50	0.55	0.60	0.65	0.70	0.75	0.80	0.85	0.90
1	Obj	NN	4.25	4.22	4.20	4.17	4.15	4.12	4.08	4.06	4.04	4.03	4.02
		Kernel	0.12	0.08	0.06	0.04	0.02	0.00	0.00	0.00	0.00	0.00	0.00
	Infeas	NN	0	0	0	0	0	0	0	0	0	0	0
		Kernel	0	0	0	0	0	0	0	0	0	0	0
2	Obj	NN	4.11	4.09	4.07	4.05	4.02	4.00	3.97	3.95	3.92	3.92	3.89
		Kernel	0.01	0.00	0.00	0.00	0.00	0.00	0.00	0.00	0.00	0.00	0.00
	Infeas	NN	26	22	0	0	0	0	0	0	0	0	0
		Kernel	0	0	0	0	0	0	0	0	0	0	0
3	Obj	NN	2.55	2.53	2.50	2.48	2.46	2.43	2.40	2.37	2.33	2.32	2.30
		Kernel	0.01	0.00	0.00	0.00	0.00	0.00	0.00	0.00	0.00	0.00	0.00
	Infeas	NN	0	0	0	0	0	0	0	0	0	0	0
		Kernel	0	0	0	0	0	0	0	0	0	0	0
4	Obj	NN	3.68	3.65	3.62	3.60	3.56	3.54	3.52	3.48	3.44	3.43	3.40
		Kernel	0.49	0.46	0.44	0.41	0.39	0.35	0.31	0.27	0.24	0.18	0.09
	Infeas	NN	1	0	0	0	0	0	0	0	0	0	0
		Kernel	0	0	0	0	0	0	0	0	0	0	0
5	Obj	NN	3.22	3.21	3.19	3.17	3.15	3.14	3.13	3.11	3.08	2.99	2.97
		Kernel	0.00	0.00	0.00	0.00	0.00	0.00	0.00	0.00	0.00	0.00	0.00
	Infeas	NN	0	0	0	0	0	0	0	0	0	0	0
		Kernel	0	0	0	0	0	0	0	0	0	0	0
6	Obj	NN	3.47	3.45	3.42	3.39	3.37	3.35	3.30	3.28	3.24	3.22	3.21
		Kernel	0.17	0.13	0.11	0.10	0.09	0.07	0.05	0.02	0.00	0.00	0.00
	Infeas	NN	0	0	0	0	0	0	0	0	0	0	0
		Kernel	0	0	0	0	0	0	0	0	0	0	0
7	Obj	NN	3.33	3.31	3.30	3.27	3.26	3.24	3.23	3.21	3.19	3.18	3.17
		Kernel	0.32	0.31	0.29	0.28	0.27	0.25	0.24	0.22	0.20	0.17	0.11
	Infeas	NN	47	41	30	27	20	14	12	9	6	4	0
		Kernel	0	0	0	0	0	0	0	0	0	0	0
8	Obj	NN	3.11	3.09	3.07	3.04	3.01	2.99	2.96	2.94	2.91	2.89	2.88
		Kernel	0.32	0.30	0.28	0.26	0.23	0.21	0.20	0.18	0.15	0.10	0.06
	Infeas	NN	0	0	0	0	0	0	0	0	0	0	0
		Kernel	0	0	0	0	0	0	0	0	0	0	0
9	Obj	NN	3.13	3.11	3.10	3.08	3.07	3.06	3.05	3.04	3.04	3.04	3.03
		Kernel	0.05	0.04	0.02	0.02	0.01	0.00	0.00	0.00	0.00	0.00	0.00
	Infeas	NN	5	3	2	2	2	0	0	0	0	0	0
		Kernel	0	0	0	0	0	0	0	0	0	0	0
10	Obj	NN	2.60	2.57	2.55	2.52	2.50	2.47	2.44	2.41	2.37	2.37	2.36
		Kernel	0.51	0.49	0.47	0.44	0.43	0.40	0.39	0.37	0.35	0.30	0.24
	Infeas	NN	0	0	0	0	0	0	0	0	0	0	0
		Kernel	0	0	0	0	0	0	0	0	0	0	0

Table 5: Feasibility vs objective on Polyhedral data in experiment 2.